Electronic fine structure calculation of metal complexes with three-open-shell *s, d, and p* configurations

Harry Ramanantoanina[1] · Claude Daul[2]

Abstract The ligand field density functional theory (LFDFT) algorithm is extended to treat the electronic structure and properties of systems with three-open-shell electron configurations, exemplified in this work by the calculation of the core and semi-core 1*s*, 2*s*, and 3*s* one-electron excitations in compounds containing transition metal ions. The work presents a model to non-empirically resolve the multiplet energy levels arising from the three-open-shell systems of non-equivalent *ns*, 3*d*, and 4*p* electrons and to calculate the oscillator strengths corresponding to the electric-dipole $3d^m \rightarrow ns^1 3d^{-m} 4p^1$ transitions, with $n = 1, 2, 3$ and $m = 0, 1, 2, \ldots, 10$ involved in the *s* electron excitation process. Using the concept of ligand field, the Slater-Condon integrals, the spin-orbit coupling constants, and the parameters of the ligand field potential are determined from density functional theory (DFT). Therefore, a theoretical procedure using LFDFT is established illustrating the spectroscopic details at the atomic scale that can be valuable in the analysis and characterization of the electronic spectra obtained from X-ray absorption fine structure or electron energy loss spectroscopies.

✉ Harry Ramanantoanina
harry.ra@hotmail.com

Claude Daul
claude.daul@unifr.ch

[1] Paul Scherrer Institute, CH-5232 Villigen, Switzerland

[2] Department of chemistry, University of Fribourg, Chemin du musée 9, CH-1700 Fribourg, Switzerland

Introduction

Ligand field theory is a very successful concept in describing the bonding regime and the electronic properties of transition metal as well as rare-earth ions in coordination compounds with or without open-shells [1–5]. It is a phenomenological model developed 80 years ago in the work of John Hasbrouck van Vleck [6] and Hans Bethe [7]. At the very beginning ligand field theory was operated with only empirical parameters [6, 7]. However in the last few decades, the ligand field concept was often used in conjunction with first principles modeling studies either at the wavefunction [8–10] or density functional levels of theory [11–15]. The important growth of computational technics also has a non-negligible impact on the development of non-empirical ligand field calculation. Twenty years ago, the original paper of Claude Daul and Mihail Atanasov [16] set the basis of the ligand field and density functional theory (DFT) calculation, which is named by the acronyms LFDFT. The theoretical model, operated only with single-open-shell of *d* or *f* electrons, has solved chemistry problems related to electron structure effect such as zero field splitting (ZFS) [17, 18], Zeeman interaction, hyper-fine splitting (HFS) [19], magnetic exchange coupling [14, 20], shielding constants [21, 22] etc. The motivation for this theoretical model itself was the explicit treatment of near degeneracy correlation using ad hoc configuration interaction within the active space of the Kohn-Sham molecular orbitals with dominant *d* or *f* character [16]. This configuration interaction treatment is based on a symmetry decomposition in the full rotation group and on a ligand field analysis of the energies of

all the single determinant (microstates) arising from this active space expressed by means of first principles DFT calculations. The computational innovation at this stage of the model development consists of the formulation of the multi-determinental concept in DFT using the average of configuration (AOC) approach [16], i.e., the active space is fundamentally distinguished within an AOC occupation of frozen Kohn-Sham molecular orbitals (KS), eventually with fractional occupations of the d or f orbitals.

Recently (cf. the work of Harry Ramanantoanina et al. [23–28]), the LFDFT method was extended to handle the electronic structure and properties arising from two-open-shell electron configurations for the description of the photophysical properties of lanthanide based phosphors. Presently, the LFDFT is again extended in this work to account for the electronic structure and properties arising from excited three-open-shell electron configurations resulting, in principle, from the excitations of core or semi-core electrons, which are visible in soft or hard regime X-ray absorption fine structure spectroscopy [29–35] as well as in energy loss spectroscopy [36, 37].

Herein we present a fully theoretical work based on LFDFT to solve non-empirically the multiplet structure arising from three-open-shell electron configurations. The model is illustrated by the calculation of the electronic structures and properties of transition metal compounds considering the excited $ns^13d^m4p^1$ electron configuration, with $n = 1, 2, 3$ and $m = 0, 1, 2, …, 10$. More especially, we study the transition metal Mn^{2+} ion as well as the complex $(Mn(H_2O)_6)^{2+}$ in providing a detailed analysis of the spectroscopy and the microscopic origin of the core and semi-core $1s$ or $2s$ or $3s$ one-electron excitation process. Hence, the oscillator strengths of the electric-dipole allowed $3d^5 \rightarrow ns^13d^54p^1$ transitions of Mn^{2+} in the free ion and in the complex $(Mn(H_2O)_6)^{2+}$ are calculated. The results can be used as reference studies to analyze and to characterize experimental spectra obtained from X-ray absorption or electron energy loss spectroscopies. The choice of the Mn^{2+} ion and its aqua complex has practical reasons. First, the ground electron configuration of Mn^{2+} is $3d^5$, giving rise to the largest possible ligand field Hamiltonian in this system. Moreover, the atomic structure of the complex $(Mn(H_2O)_6)^{2+}$ has a high symmetrical cubic arrangement, belonging to the T_h point group. This is further comforted by the high-spin (^6A_g) ground state of Mn^{2+} in this compound, making any possible Jahn-Teller distortion [38, 39] negligible. Eventually, the presence of the inversion center in the T_h point group allows us to neglect the impact of the $3d^5 \rightarrow ns^13d^6$ transitions, although they can also be calculated by means of the LFDFT. These transitions are strictly speaking not electric-dipole allowed, but they are often visible in the observed X-ray absorption spectra of transition metal compounds [40–43], more importantly when non-centro-symmetric objects are investigated. [44–47].

Methods

The DFT calculations were carried out by means of the Amsterdam Density Functional (ADF) program package (ADF2014.01) [48–50]. We stress that ADF is a DFT code that has the set of keywords facilitating the AOC calculations and Slater determinant emulation needed by the LFDFT procedure [16]. The local density approximation (LDA) functional SVWN [51] was used to determine the geometry of the complex $(Mn(H_2O)_6)^{2+}$. The electronic ground state of this complex belongs to the ^6A_g term originating from the $3d^5$ electron configuration of Mn^{2+}. Therefore the minimum energy structure is obtained by unrestricted self-consistent-field (SCF) calculation constraining the spin multiplicity to six and the atomic structure of the complex to the T_h point group. The optimized minimum energy structure of $(Mn(H_2O)_6)^{2+}$ results bond distances (in Å) of 2.0978 and 0.9785 for Mn–O and O–H, respectively. Then based on this LDA minimum energy structure, the generalized gradient approximation (GGA) functional (PBE) [52] was used to compute the electronic structure related to the ground $3d^5$ and the excited $ns^13d^54p^1$ electron configurations of Mn^{2+}, with $n = 1, 2, 3$, in the free ion as well as in the aqua-complex and the related optical properties. Following the LFDFT procedure [16, 28], the Slater-Condon integrals, the spin-orbit coupling constants, and the ligand field parameters are obtained from the radial functions and the eigenvalues of the molecular Kohn-Sham orbitals having dominant $1s$, $2s$, $3s$, $3d$, and $4p$ characters.

The LFDFT, which will be available soon in the ADF program package [48–50], implies single-point restricted SCF calculations without symmetry constraint (C_1 point group) based on a minimum energy atomic structure with equal smearing of electrons to represent the electron configuration systems. This is achieved by AOC occupation schemes, where we insure that five electrons are evenly distributed in the $3d$ orbitals of Mn^{2+} to comply with the ligand field concept [16, 28] considering the ground electron configuration, whereas one electron is promoted from the core and semi-core $1s$ or $2s$ or $3s$ orbitals and is evenly distributed in the $4p$ orbitals considering the excited electron configurations. The molecular orbitals were expanded using triple-zeta plus two polarization Slater-type orbital (STO) functions (TZ2P+) for the manganese atoms and triple-zeta plus one polarization STO function (TZP) for the oxygen and hydrogen atoms.

Results and discussion

The ligand field master equation allows representation of the effective Hamiltonian operator with respect to quantum effects due to electron-electron repulsion and exchange (H_{ER}), spin-

orbit coupling interaction (H_{SO}), and ligand field splitting (H_{LF}):

$$H = H_0 + H_{ER} + H_{SO} + H_{LF} \qquad (1)$$

where, the matrix elements of H (Eq. 1) are expressed on the basis of single determinants of spin-orbitals (Slater-determinants) arising from the electron configuration of multiple-open-shell systems, for example in the present studies of $ns^1 3d^m 4p^1$ configurations, with $n = 1, 2, 3$ and $m = 1, 2, \ldots, 10$. The diagonalization of H yields eigenvalues also known as multiplet energy levels arising from the electron configuration from which the effective Hamiltonian operates.

The term for the electron-electron repulsion and exchange in Eq. 1 is based on the central-field approximation and perturbation theory of Slater: [53, 54]

$$
\begin{aligned}
H_{ER} = &\sum_{k=2,4} F^k(dd) f_k(dd) + F^2(pd) f_2(pd) \\
&+ \sum_{k=1,3} G^k(pd) g_k(pd) + G^1(sp) g_1(sp) \\
&+ G^2(sd) g_2(sd)
\end{aligned}
\qquad (2)
$$

where, the matrix elements of H_{ER} are constructed in terms of the Slater-Condon integrals F and G representing the Coulomb and exchange interactions, respectively; and the angular coefficient f and g (Eq. 2). [53–55].

Eq. 2 is valid for any system belonging to the present $s^1 d^m p^1$ electron configuration but it can be extended to account for any three-open-shell systems by providing appropriate supplementary terms, which represent both Coulomb and exchange electron repulsions within two shells. Note that the zeroth order Slater-Condon parameters $F^0(sp)$, $F^0(dp)$, $F^0(ss)$, $F^0(dd)$, and $F^0(sd)$ are omitted in Eq. 2 because they are already merged with the term H_0 present in Eq. 1, whose matrix elements are diagonal:

$$
H_0 = \begin{pmatrix} I_{N(3d^m)} \cdot 0 & (0) \\ (0) & I_{N(ns^1 3d^m 4p^1)} \cdot \Delta \end{pmatrix}
\qquad (3)
$$

where, Δ is the parameter, which represents the energy gap between the ground ($3d^m$) and excited ($ns^1 3d^m 4p^1$) electron configurations. Δ is calculated from DFT as the difference between the total electronic energies of the complex having the excited and the ground electron configurations. The analytical form of Δ depends on the number of valence electrons present in the d orbitals (i.e., the constant m), for instance for $m = 5$ we obtain the following:

$$
\begin{aligned}
\Delta = &h_p - h_s + F^0(sp) + 5F^0(dp) - F^0(ss) - 5F^0(sd) \\
&+ B_0^0(pp) - B_0^0(ss) + \Delta^0(dd)
\end{aligned}
\qquad (4)
$$

where, h_p and h_s are one-electron terms corresponding to the kinetic and electron-nuclear energies and $\Delta^0(dd)$ is the variation of the quantity $h_d + 10F^0(dd) + B^0{}_0(dd)$ in the excited $ns^1 3d^5 4p^1$ and the ground $3d^5$ electron configurations. The B parameters represent the ligand field interaction, which will be discussed in next paragraph. We note that Δ contains many different terms (Eq. 4), although those terms cannot be discriminated separately from the DFT calculation.

In Eq. 3, I_N is an identity matrix of rank N; and N represents the dimension of the Hilbert space given by the total number of single determinants of spin-orbitals arising from the multiple-open-shell electron configurations. The dimension N is determined using combinatoric formulas. In the ground d^m configuration, N can be determined as follows:

$$
N(3d^m) = \begin{pmatrix} 10 \\ m \end{pmatrix}
\qquad (5)
$$

with respect to the number (m) of valence electrons present in the d orbitals. On the other hand in the excited $ns^1 3d^m 4p^1$ configuration, independent of the n value we obtain a more complicated formula, which takes into consideration three non-equivalent electrons in s, d, and p shells:

$$
N(ns^1 3d^m 4p^1) = \begin{pmatrix} 2 \\ 1 \end{pmatrix} \begin{pmatrix} 10 \\ m \end{pmatrix} \begin{pmatrix} 6 \\ 1 \end{pmatrix}
\qquad (6)
$$

The calculated values of $N(ns^1 3d^m 4p^1)$ are listed in Table 1 considering $m = 0, 1, 2, \ldots, 10$; together with the generated spectral terms due to the atomic contribution (H_{ER}) in the ligand field Hamiltonian. The number of Slater-determinants reaches its highest values for the $ns^1 3d^5 4p^1$ system with 3024 microstates, whose calculation is feasible within the actual status of the LFDFT algorithm. We do not list in Table 1 the calculated values of $N(3d^m)$ together with the related spectral terms since they are well known, and easily found elsewhere in textbooks [56, 57].

The term for the spin-orbit coupling interaction in Eq. 1 is obtained as the product of one-electron spin-orbit coupling constants ζ_{3d} and ζ_{4p}, calculated by means of the zeroth order regular approximation (ZORA) implemented in the ADF program package [48–50], with angular coefficients (d_d and d_p), which depend on the spin and angular momentum operators defined in terms of spherical harmonics of order $l = 2$ and $l = 1$ for the d and p electrons, respectively:

$$
H_{SO} = \zeta_{3d} d_d + \zeta_{4p} d_p
\qquad (7)
$$

The spin-orbit coupling interaction transforms the spectral terms presented in Table 1 into spin-orbit components. For example, the energies of the ^3P state belonging to the $ns^1 3d^0 4p^1$, $ns^1 3d^2 4p^1$ and $ns^1 3d^4 4p^1$ electron configurations (see Table 1) will be split by spin-orbit into $^3P_0$, $^3P_1$, and $^3P_2$ levels.

The term for the ligand field splitting in Eq. 1 represents the contribution of the chemical environment of the metal ion on the electronic structure. We use the Wybourne formalism [58]

Table 1 All multiplets and number of microstates N corresponding to the excited $ns^1 3d^m 4p^1$ electron configurations of transition metal ions with any value of n and m

Configuration	N	Spectral terms[a]
$ns^1 3d^0 4p^1$ and $ns^1 3d^{10} 4p^1$	12	^{1}P & ^{3}P
$ns^1 3d^1 4p^1$ and $ns^1 3d^9 4p^1$	120	$2 \times \,^2$P, $2 \times \,^2$D, $2 \times \,^2$F, ^{4}P, ^{4}D & ^{4}F
$ns^1 3d^2 4p^1$ and $ns^1 3d^8 4p^1$	540	^{1}S, $3 \times \,^1$P, $2 \times \,^1$D, $3 \times \,^1$F, $2 \times \,^1$G, ^{1}H, $2 \times \,^3$S, $4 \times \,^3$P, $5 \times \,^3$D, $4 \times \,^3$F, $3 \times \,^3$G, ^{3}H, ^{5}S, ^{5}P, $2 \times \,^5$D, ^{5}F & ^{5}G
$ns^1 3d^3 4p^1$ and $ns^1 3d^7 4p^1$	1440	$3 \times \,^2$S, $7 \times \,^2$P, $10 \times \,^2$D, $9 \times \,^2$F, $7 \times \,^2$G, $4 \times \,^2$H, $2 \times \,^2$I, $3 \times \,^4$S, $5 \times \,^4$P, $8 \times \,^4$D, $6 \times \,^4$F, $5 \times \,^4$G, $2 \times \,^4$H, ^{4}I, ^{6}S, ^{6}P, $2 \times \,^6$D & ^{6}G
$ns^1 3d^4 4p^1$ and $ns^1 3d^6 4p^1$	2520	$2 \times \,^1$S, $7 \times \,^1$P, $8 \times \,^1$D, $9 \times \,^1$F, $7 \times \,^1$G, $5 \times \,^1$H, ^{1}I, ^{1}K, $4 \times \,^3$S, $10 \times \,^3$P, $14 \times \,^3$D, $14 \times \,^3$F, $11 \times \,^3$G, $7 \times \,^3$H, $4 \times \,^3$I, ^{3}K, $2 \times \,^5$S, $5 \times \,^5$P, $7 \times \,^5$D, $6 \times \,^5$F, $4 \times \,^5$G, $2 \times \,^5$H, ^{5}I, ^{7}P, ^{7}D & ^{7}F
$ns^1 3d^5 4p^1$	3024	$3 \times \,^2$S, $12 \times \,^2$P, $15 \times \,^2$D, $17 \times \,^2$F, $12 \times \,^2$G, $9 \times \,^2$H, $4 \times \,^2$I, $2 \times \,^2$K, $2 \times \,^4$S, $10 \times \,^4$P, $11 \times \,^4$D, $13 \times \,^4$F, $9 \times \,^4$G, $6 \times \,^4$H, $2 \times \,^4$I, ^{4}K, ^{6}S, $4 \times \,^6$P, $3 \times \,^6$D, $3 \times \,^6$F, $2 \times \,^6$G, ^{6}H & ^{8}P

[a] for all entries in the table, the number in front of the spectral terms (e.g., $3 \times \,^2$S) denotes the multiple occurrence of the multiplet ^{2}S in this electron configuration

with the Wybourne-normalized crystal field parameters B and the spherical harmonic tensor operator C acting only on the d and p orbitals:

$$H_{LF} = \sum_{k=0,2,4} \sum_{q=-k}^{k} B_q^k(dd) C_q^{(k)} + \sum_{k=0,2} \sum_{q=-k}^{k} B_q^k(pp) C_q^{(k)} +$$
$$+ \sum_{k=1,3} \sum_{q=-k}^{k} B_q^k(pd) C_q^{(k)} + \sum_{q=-2}^{2} B_q^2(sd) C_q^{(2)} \quad (8)$$

The expansion of the ligand field potential in terms of the spherical harmonics basis (Eq. 7) is always limited by symmetry constraint [59]. In the present studies of aqua complexes of transition metal ions (see Introduction) belonging to the high symmetrical T_h point group (see Fig. 1), only the parameter $B^4_0(dd)$ is significant (Eq. 9) [59]. The s and p orbitals belong to the a_g and the threefold degenerate t_u irreducible representations (*irreps*) of the T_h point group, respectively, i.e., their energies are not split by the ligand field effect. On the other hand, the d orbitals belong to the e_g and t_g irreps. Their energies are split by ligand field effect into two groups forming the basis of the t_g and e_g irreps, which are constituted by (d_{xy}, d_{xz}, d_{yz}) and (d_{z2}, d_{x2-y2}) components of the $3d$ orbitals, respectively. In Eq. 9, the parameters of the ligand field potential are calculated using the quantities $<e_g|H_{LF}|e_g>$ and $<t_g|H_{LF}|t_g>$ representing the energies of the e_g and t_g molecular Kohn-Sahm orbitals of dominant $3d$ characters of Mn^{2+} obtained from DFT.

$$B_0^4(dd) = \frac{21}{10} \left(\langle e_g|H_{LF}|e_g \rangle - \langle t_g|H_{LF}|t_g \rangle \right) \quad (9)$$

In this work, the Slater-Condon parameters are determined non-empirically from the radial functions of the Kohn-Sham orbitals with dominant $1s$, $2s$, $3s$, $3d$, and $4p$ characters. We

must point out that the shape of the radial function is strongly dependent on the ligand field potential, a phenomenology commonly recognized by the term nephelauxetic effect [60]. Depending to the bonding regime between the $3d$ orbitals and the ligands, we obtain five types of radial functions for R_{3d}. In principle, they all have identical symmetry and they correspond to the calculated radial functions for the $3d_{xy}$, $3d_{xz}$, $3d_{yz}$, $3d_{z2}$, and $3d_{x2-y2}$ components of the $3d$ orbitals. In Fig. 2, the radial functions of molecular orbitals with dominant $3d$ characters of Mn^{2+} in the free ion and in the complex $(Mn(H_2O)_6)^{2+}$ are presented. In the free ion, the five radial functions are all equivalent since the energies of the fivefold $3d$ orbitals are degenerate. On the other hand in the complex, we obtain two different sets of radial functions as illustrated in Fig. 2 with respect to the blue and the green colored curves.

In Fig. 2, the blue curves represent R_{3dxy}, R_{3dyz}, and R_{3dxz} forming the basis of the t_g molecular orbitals whereas the
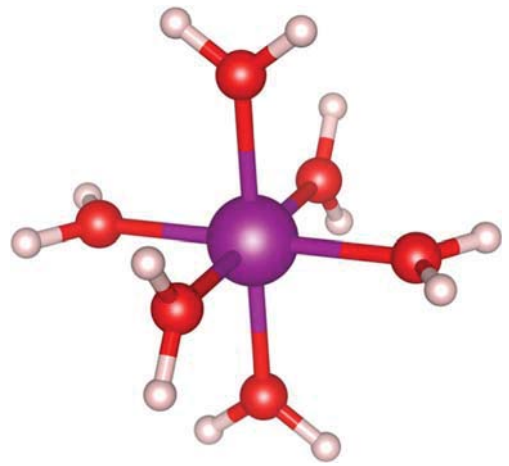

Fig. 1 Schematic representation of the complex $(Mn(H_2O)_6)^{2+}$ belonging to the T_h point group. Color code: Mn^{2+} in violet, O in red, and H in blank
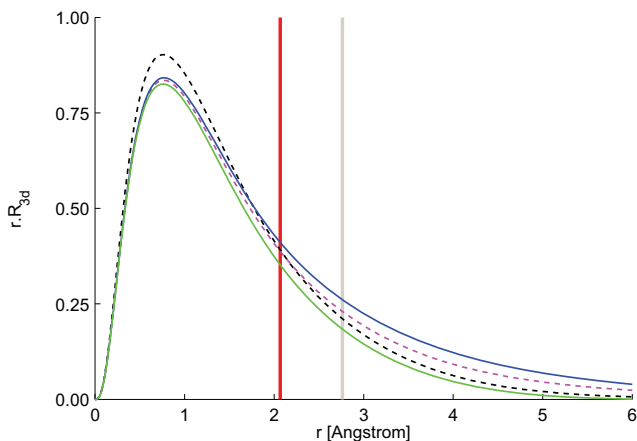
4

Fig. 2 Representation of the radial functions R_{3dxy}, R_{3dyz}, R_{3dxz}, R_{3dz2}, and $R_{3dx2-y2}$ corresponding to the molecular Kohn–Sham orbitals with dominant $3d$ characters of Mn^{2+} in the free ion (dashed black curve) and in the complex $(Mn(H_2O)_6)^{2+}$ (solid green and blue curves) obtained from an AOC calculation within the ground $3d^5$ electron configuration. The dashed magenta curve represents the average radial function R_{3d} used for the LFDFT calculations (see text). The red and gray lines represent the emplacement of the oxygen ligands and hydrogen atoms with respect to the Mn^{2+} central ion

green curves represent R_{3dz2}, and $R_{3dx2-y2}$ part of the e_g. Therefore we have to construct an average radial function R_{3d} illustrated in Fig. 2 by the dashed magenta curve, which complies with the principle of ligand field theory. [16, 28]. With this, for the ground electron configurations containing d electrons only, the following Slater-Condon parameters are requested: $F^2(dd)$ and $F^4(dd)$. They are calculated with resepct to the averaged radial function R_{3d} (see Fig. 2) obtained from DFT AOC calculation of the ground electron configuration of Mn^{2+} by means of Eq. 10.

$$F^k(dd) = \int_0^\infty \int_0^\infty \frac{r_<^k}{r_>^{k+1}} R_{3d}^2(r_1) R_{3d}^2(r_2) r_1^2 r_2^2 dr_1 dr_2 \qquad (10)$$

The calculated $F^2(dd)$ and $F^4(dd)$ parameters together with the spin-orbit coupling constant ζ_{3d} and the parameter $B^4_0(dd)$ are listed in Table 2 for Mn^{2+} in the free ion and in the complex $(Mn(H_2O)_6)^{2+}$ obtained from DFT AOC calculation of the ground $3d^5$ electron configuration of Mn^{2+}. The nephelauxetic constants β [60], which represent the ratio between the calculated parameters in the complex and in the free ion, are also listed in Table 2. Using the parameters in Table 2, we obtain the following energies for the absorption bands of d-d transitions (in eV) of $(Mn(H_2O)_6)^{2+}$ (for clarity and for comparison with available experimental results, we use the *irreps* of the O point group and drop the terms from spin-orbit coupling interaction): 0.0000 ($^6A_1$), 2.1175 ($^4T_1$), 2.6901 ($^4T_2$), 3.0646 ($^4A_1$, ^4E), 3.5373 ($^4T_2$), 3.8248 (^4E), 4.2922 ($^4T_1$). The experimental deduced energies (in eV) are: 0.0000 ($^6A_1$), 2.3311 ($^4T_1$), 2.8642 ($^4T_2$), 3.0998 and 3.1308 ($^4A_1$, ^4E), 3.4842 ($^4T_2$), 3.6826 (^4E), 4.0670 ($^4T_1$)

Table 2 Calculated parameters for the Slater–Condon integrals, the spin–orbit coupling constants and the ligand field potential (in eV) corresponding to the ground single-open-shell $s^2 d^5 p^0$ electron configurations of Mn^{2+} in free ion and in the complexes $(Mn(H_2O)_6)^{2+}$; together with the nephelauxetic constant β (in [−])

	Free Mn^{2+} ion	Mn^{2+} in $(Mn(H_2O)_6)^{2+}$	β
$F^2(dd)$	9.8478	8.0916	0.8217
$F^4(dd)$	6.0964	4.9860	0.8179
ζ_{3d}	0.0744	0.0659	0.8858
$B_0^4(dd)$	-	2.5706	-

[56, 57]. Although we notice a slight shift of these energy levels, the overall agreement between the theoretical and experimental results (vide supra) is very encouraging.

For the excited electron configurations containing s, d, and p non-equivalent electrons, the following Slater-Condon parameters are left: $G^1(sp)$, $G^2(sd)$, $F^2(dp)$, $G^1(dp)$, $G^3(dp)$, $F^2(dd)$, and $F^4(dd)$. The term $F^2(pp)$ is dropped since the p orbitals accommodate only one electron in this work, which is not the case if two or more electrons are placed in the orbitals. The parameters $F^2(dd)$ and $F^4(dd)$ are calculated using Eq. 10 but with the averaged radial function R_{3d} obtained from DFT AOC calculation of the excited electron configuration of Mn^{2+}. We present, in Fig. 3, the average radial functions R_{1s}, R_{2s}, R_{3s}, R_{3d}, and R_{4p} of the Kohn-Sham orbitals with dominant $1s$, $2s$, $3s$, $3d$, and $4p$ characters of Mn^{2+} in the free ion and in the complex $(Mn(H_2O)_6)^{2+}$. These radial functions (Fig. 3) are calculated from DFT using the AOC occupation scheme evenly distributing one electron in the $1s$ or $2s$ or $3s$ orbitals, five electrons in the $3d$, and one electron in the $4p$. Therefore, we note that R_{3d} differs from the excited ($ns^1 3d^5 4p^1$) to the ground ($3d^5$) electron configurations leading to different values of the parameters listed in Table 3.

The parameters $G^1(sp)$ and $G^2(sd)$ represent the repulsion of electrons in the open-shell $1s$ or $2s$ or3 s orbitals with the $4p$ and $3d$, respectively. They are calculated in terms of the average radial functions R_{1s}, R_{2s}, R_{3s}, R_{4p}, and R_{3d} obtained from DFT AOC calculation of the excited electron configuration of Mn^{2+} (Fig. 3) by means of Eq. 11 and Eq. 12.

$$G^1(sp) = \int_0^\infty \int_0^\infty \frac{r_<}{r_>^2} R_{ns}(r_1) R_{4p}(r_2) R_{4p}(r_1) R_{ns}(r_2) r_1^2 r_2^2 dr_1 dr_2 \qquad (11)$$

$$G^2(sd) = \int_0^\infty \int_0^\infty \frac{r_<^2}{r_>^3} R_{ns}(r_1) R_{3d}(r_2) R_{3d}(r_1) R_{ns}(r_2) r_1^2 r_2^2 dr_1 dr_2 \qquad (12)$$

In the simplest case of $s^1 d^0 p^1$ system (Table 1), the energy separation between the ^1P and ^3P states represent 2/3 of the value of $G^1(sp)$. The calculated values of $G^1(sp)$ and $G^2(sd)$
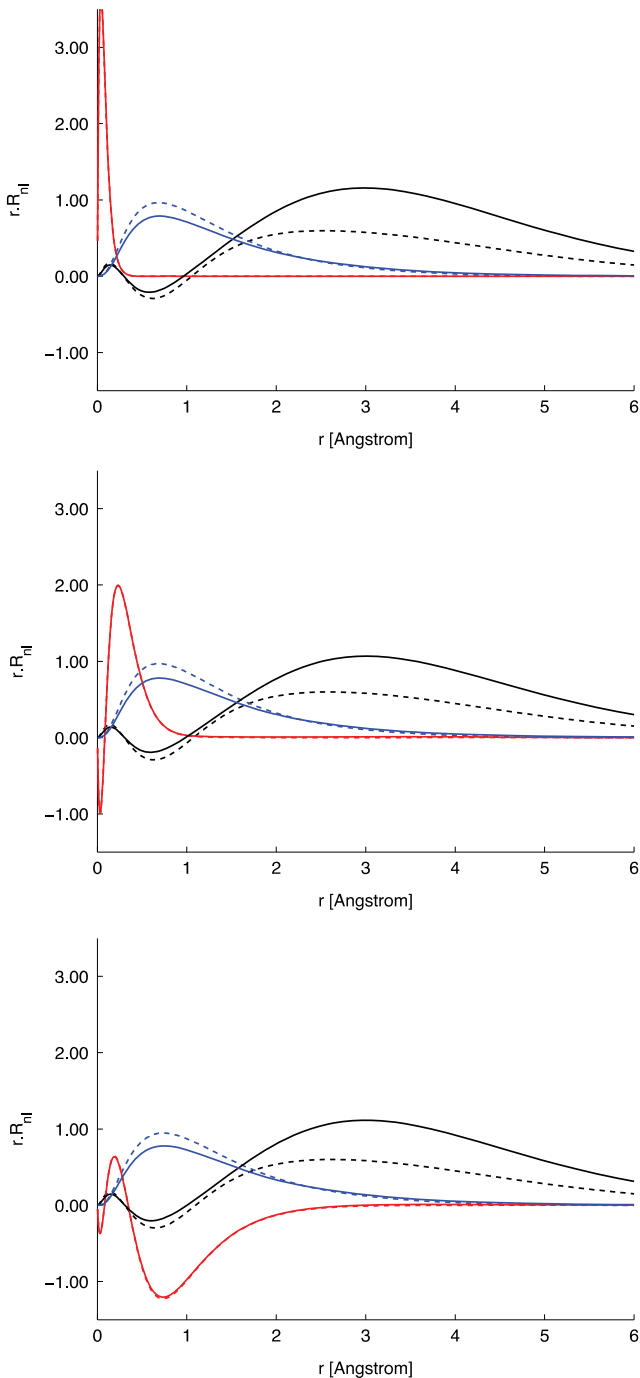
Fig. 3 Representation of the radial wavefunctions R_{ns} (in red) with $n = 1$ (top), 2 (middle), and 3 (botton), R_{3d} (in blue) and R_{4p} (in black) corresponding to the molecular Kohn–Sham orbitals with dominant $1s$, $2s$, $3s$, $3d$, and $4p$ characters of Mn^{2+} in the free ion (dashed-curves) and in the complex $(Mn(H_2O)_6)^{2+}$ (solid curves) obtained from AOC calculations with $1s^1 3d^5 4p^1$ (top), $2s^1 3d^5 4p^1$ (middle), and $3s^1 3d^5 4p^1$ (bottom) electron configurations

They are calculated in terms of the average radial functions R_{4p} and R_{3d} in Fig. 3 by means of Eq. 13 and Eq. 14.

$$F^2(dp) = \int_0^\infty \int_0^\infty \frac{r_<^2}{r_>^3} R_{3d}^2(r_1) R_{4p}^2(r_2) r_1^2 r_2^2 dr_1 dr_2 \qquad (13)$$

$$G^k(dp) = \int_0^\infty \int_0^\infty \frac{r_<^k}{r_>^{k+1}} R_{3d}(r_1) R_{4p}(r_2) R_{4p}(r_1) R_{3d}(r_2) r_1^2 r_2^2 dr_1 dr_2 \qquad (14)$$

The calculated values of $F^2(dp)$, $G^1(dp)$, and $G^3(dp)$ are listed in Table 3. The parameters for the ligand field potential as well as the spin-orbit coupling are also listed in Table 3 obtained from the DFT AOC calculation of the excited ($ns^1 3d^5 4p^1$) electron configuration of Mn^{2+} in the free ion and the complex $(Mn(H_2O)_6)^{2+}$. The multiplet energy levels arising from the $1s^1 3d^5 4p^1$, $2s^1 3d^5 4p^1$, and $3s^1 3d^5 4p^1$ configurations of Mn^{2+} are calculated using the quantities in Table 3, and diagonalizing the ligand field Hamiltonian (Eq. 1), with a ground state energy correction corresponding to the lowest $^6S_{5/2}$ and ^6A_g states of the $3d^5$ configuration, respectively for Mn^{2+} in the free ion and in the complex $(Mn(H_2O)_6)^{2+}$. The results are graphically represented in Fig. 3.

The mechanisms of the core s electron excitation are in principle characterized by the $3d^m \rightarrow ns^1 3d^{m+1}$ and $3d^m \rightarrow ns^1 3d^m 4p^1$ electron transitions. The $3d^m \rightarrow ns^1 3d^m 4p^1$ transitions fulfill the electric-dipole selection rules because of the mixing between s and p electrons. However, the $3d^m \rightarrow ns^1 3d^{m+1}$ transitions are electric-quadrupole allowed, resulting in principle to very small intensities relative to the dipole ones [31, 56]. However, we note that the $3d^m \rightarrow ns^1 3d^{m+1}$ transitions are often visible in the spectra of non-centro-symmetric compounds [40–47]. The possible mixing between the $3d$ orbitals with the $4p$ virtuals ensures a dipole character on the electron transition mechanism. This is not discussed here since $(Mn(H_2O)_6)^{2+}$ belongs to the high symmetric T_h point group.

The intensities of the $3d^5 \rightarrow ns^1 3d^5 4p^1$ transitions are calculated by means of the matrix elements of the electric dipole moment operator D (Eq. 15). D is the product between a radial integral involving the radial function R_{ns} and R_{4p} of Kohn-Sham orbitals of dominant ns and $4p$ characters (Fig. 3), and an angular integral, which can be associated with the Clebsh-Gordan coefficients: [56]

$$D_\mu = \frac{\sqrt{4\pi}}{3} \langle R_{ns}|r|R_{4p}\rangle \langle Y_{0,0}|Y_{1,\mu}|Y_{4,mp}\rangle \qquad (15)$$

D (Eq. 15) is used for the computation of the oscillator strengths related to the $3d^5 \rightarrow ns^1 3d^5 4p^1$ transitions, by distributing its elements over the whole manifold of the multi-electronic configuration interaction obtained from the ligand field Hamiltonian (Eq. 1). In the free ion case, the oscillator strengths are calculated taking as initial state the six-fold

are listed in Table 3 considering Mn^{2+} in the free ion and in the complex $(Mn(H_2O)_6)^{2+}$.

The parameters $F^2(dp)$, $G^1(dp)$, and $G^3(dp)$ represent the repulsion of electrons in the open-shells $3d$ and $4p$ orbitals.

Table 3 Calculated parameters for the Slater–Condon integrals, the spin–orbit coupling constants, and the ligand field potential (in eV) corresponding to the excited three-open-shell $1s^1 3d^5 4p^1$, $2s^1 3d^5 4p^1$, and $3s^1 3d^5 4p^1$ electron configurations of Mn^{2+} in free ion and in the complex $(Mn(H_2O)_6)^{2+}$

	Free Mn^{2+} ion			Mn^{2+} in $(Mn(H_2O)_6)^{2+}$		
	$1s^1 3d^5 4p^1$	$2s^1 3d^5 4p^1$	$3s^1 3d^5 4p^1$	$1s^1 3d^5 4p^1$	$2s^1 3d^5 4p^1$	$3s^1 3d^5 4p^1$
$F^2(dd)$	10.8368	10.9056	10.6063	5.1868	4.9245	5.1942
$F^4(dd)$	6.7480	6.8017	6.6137	3.2127	3.0536	3.2221
Δ	6559.7	759.0	92.46	6556.6	755.8	90.30
$G^1(sp)$	0.2253	0.1646	0.5746	0.1707	0.1059	0.3593
$G^2(sd)$	0.0470	4.5975	11.1951	0.0312	2.9915	7.5041
$F^2(dp)$	2.1957	2.1253	2.2589	3.8297	3.0547	3.7602
$G^1(dp)$	0.9047	0.8356	0.9248	1.7833	1.3728	1.7958
$G^3(dp)$	0.7752	0.7269	0.7965	1.2435	0.9636	1.2508
ζ_{3d}	0.0946	0.0945	0.0818	0.0634	0.0614	0.0555
ζ_{4p}	0.0822	0.0786	0.0791	0.0623	0.0509	0.0557
$B_0^4(dd)$	-	-	-	2.4843	2.4822	2.6985

degenerate $^6S_{5/2}$ state originating from the $3d^5$ electron configuration of Mn^{2+}. In the complex $(Mn(H_2O)_6)^{2+}$ case, the initial state consists of the ^6A_g ground state of the $3d^5$ electron configuration of Mn^{2+}, whose energy is split by a very small zero field splitting (in the magnitude of 10^{-4} eV). In both cases, we consider as final states the whole manifold of the $ns^1 3d^5 4p^1$ multiplets. The calculated oscillator strengths are also graphically represented in Fig. 4 using bar diagramms placed above the multiplet energy levels.

The intensity plots are in arbitrary units, i.e., normalized to unity for both oscillator strenghts and Gaussian convolution (see Fig. 4). We use the Gaussian broadening of the oscillator strengths with a half width of 0.2 eV since the model of spectral shape often depends on many factors that are not always tractable by pure first principles model [61, 62].

The calculations of the free Mn^{2+} ion show that the $3d^5 \rightarrow ns^1 3d^5 4p^1$ transitions are characterized by two major bands whose energy separation increases in terms of n (see Fig. 4, left-hand-side). The peaks originate from the transition $3d^5$ $(^6S) \rightarrow ns^1 3d^5 4p^1$ (^6P), which fulfill the electric-dipole moment selection rules. The ^6P state occurs exactly four times in the multiplet of $ns^1 3d^5 4p^1$ configurations (see Table 1). Therefore we can determine the origin of the ^6P states yielding the two highest intensities as the direct product between the ground state of $3d^5$ (i.e., ^6S) with two electrons in both s and p orbitals:

$$ns^1 3d^5 4p^1 \rightarrow {}^2S \otimes {}^6S \otimes {}^2P \rightarrow \left({}^7S + {}^5S \right) \otimes {}^2P \tag{16}$$
$$\rightarrow {}^8P + {}^6P + {}^6P + {}^4P$$

On the other hand, the two other ^6P states have intensities which are not discernable in Fig. 4. They results from the direct product between two excited states of the $3d^5$ electron configuration, namely the ^4P and ^4D states, with two electrons in both s and p orbitals. The calculations of Mn^{2+} in the complex $(Mn(H_2O)_6)^{2+}$ show that the calculated spectra of the $3d^5$

$(^6A_g) \rightarrow ns^1 3d^5 4p^1$ still conserve the free ion characters with two noticeably high intensity bands, especially for $n = 2$ and 3 (see Fig. 4, right-hand-side). It is obtained that the energy separations between these two peaks are smaller in the metal aquo-complex than in the free ion (see Fig. 4). The repulsion between the ns and $3d$ electrons of the metal ion (parameterized by the Slater-Condon $G^2(sd)$ (Eq. 12) quantities in Table 3) is mainly responsible for this energy separation. However, the smaller energy separations in the metal aquo-complex indicate that the mean distance between the electrons has increased, as results of the expansion of the radial functions of the $3d$ orbitals toward the oxygen ligands (see also Fig. 3). This expansion of the $3d$ radial functions is termed by the nephelauxetic effect [60] and results in part from the redistribution of electrons within the metal complexes, for instance due to the metal-ligand orbitals overlap. Besides, a small redistribution of the intensities is also calculated (Fig. 4, right-hand-side) due to the influence of the spin-orbit coupling interaction and the ligand field splitting on the atomic spectral terms of the excited three-open-shell $ns^1 3d^5 4p^1$ configurations.

Conclusions

We have shown that LFDFT can be used to solve the electronic structrure and properties of excited three-open-shell electron configurations. We have investigated the core and semicore s electron excitations in compounds, which contain transition metal ions taking explicitly the case of divalent manganese ion as a practical example. Using the ligand field concept, we have calculated parameters corresponding to the Slater-Condon integrals, spin-orbit coupling constants, and ligand field potential from density functional theory. Although our results are yet independent of any experimental validation, we
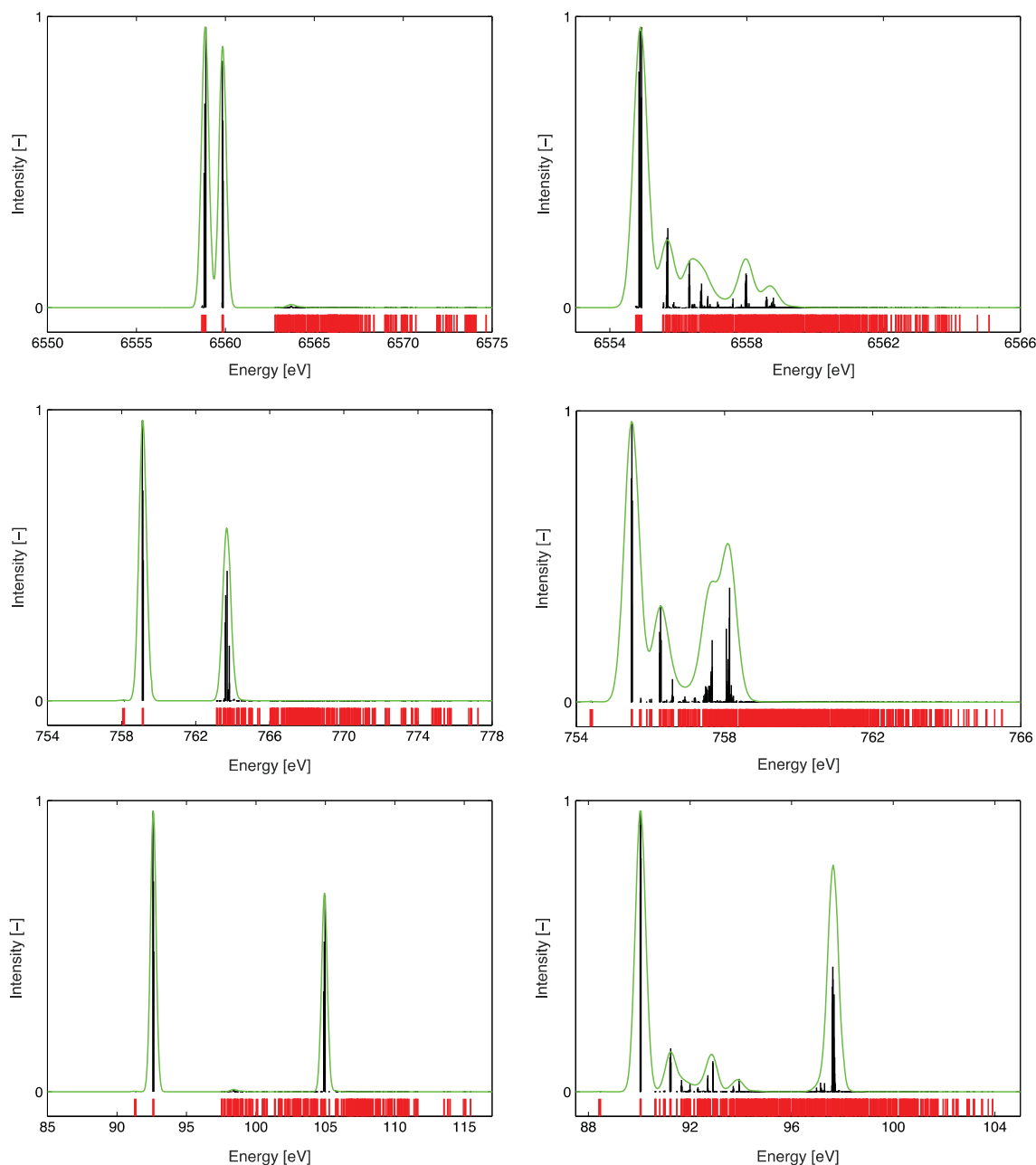
Fig. 4 Calculated multiplet energy levels (in red) arising from the excited $1s^13d^54p^1$ (in the top), $2s^13d^54p^1$ (in the middle), and $3s^13d^54p^1$ (in the bottom) electron configurations of Mn^{2+} in the free ion (in the left-hand side) and in the complex $(Mn(H_2O)_6)^{2+}$ (in the right-hand-side); together with the intensities of the absorption $3d^5$ ($^6S_{5/2}$ in the free ion and ^6A_g in the complex) $\rightarrow ns^13d^54p^1$ transitions, with $n = 1, 2, 3$, i.e., oscillator strengths (in black) of the electric-dipole allowed transitions. The green curve represents the oscillator strengths convoluted with Gaussian bands with a half width of 0.20 eV

are convinced that the combination of first principles methods with the ligand field analysis is a good way to understand the relationship between electronic structures and optical properties of materials.

With this work, we intend to show a particular aspect of doing science, which consists of developing models to describe and predict the photo-physical and magnetic properties of metal compounds with strongly correlated d and f electrons. To achieve this goal, like our friend and colleague Henry

Chermette, we frequently applied Occam's principle (cf. the English Franciscan friar William of Occam (c. 1287–1347)). Briefly, it can be interpreted as: "*Among competing hypotheses, the one with the fewest assumptions should be selected.*" The history of science is full of examples that illustrate this principle very well. In our field, the most obvious ones consist of using the resolution of the identity to calculate matrix elements in density functional theory or exploiting the symmetry invariance of the Schrödinger equation. In this Festschrift

dedicated to Henry Chermette, we are pleased to present this three-open-shell LFDFT concept to demonstrate that simple theory can solve complex problems such as the optical manifestation of non-equivalent s, d, and p electrons.

References

1. Chermette H (1998) Density functional theory: A powerful tool for theoretical studies in coordination chemistry. Coord Chem Rev 178–180:699

2. Figgis BN, Hitchman MA (2000) Ligand field theory and its applications. Wiley-VCH, New York

3. Gerloch M, Slade RC (1973) Ligand field parameters. Cambridge University Press, Cambridge

4. Newman DJ, Ng BKC (2000) Crystal field handbook. Cambridge University Press, Cambridge

5. Judd BR (1998) Operator techniques in atomic spectroscopy. Princeton University Press, Princeton

6. van Vleck JH (1935) Valence Strength and the Magnetism of Complex Salts. J Chem Phys 3:807

7. Bethe H (1929) Termaufspaltung in Kristallen. Ann Phys 395:133

8. Atanasov M, Ganyushin D, Sivalingam K, Neese F (2011) A modern first-principles view on ligand field theory through the eyes of correlated multireference wavefunctions. Struct Bond 143:149

9. Aravena D, Atanasov M, Neese F (2016) Periodic Trends in Lanthanide Compounds through the Eyes of Multireference ab Initio Theory. Inorg Chem 55:4457

10. Chilton NF, Lei H, Bryan AM, Grandjean F, Long GJ, Power PP (2015) Ligand field influence on the electronic and magnetic properties of quasi-linear two-coordinate iron(II) complexes. Dalton Trans 44:11202

11. Atanasov M, Comba P, Daul CA (2008) Combined Ligand Field and Density Functional Theory Analysis of the Magnetic Anisotropy in Oligonuclear Complexes Based on FeIII−CN−MII Exchange-Coupled Pairs. Inorg Chem 47:2449

12. Zbiri M, Atanasov M, Daul C, Garcia-Lastra J-M, Wesolowski TA (2004) Application of the density functional theory derived orbital-free embedding potential to calculate the splitting energies of lanthanide cations in chloroelpasolite crystals. Chem Phys Lett 397:441

13. Haverkort MW, Zwierzycki M, Andersen OK (2012) Multiplet ligand-field theory using Wannier orbitals. Phys Rev B 85:165113

14. Atanasov M, Daul CA (2003) A DFT based ligand field model for magnetic exchange coupling in transition metal dimmer complexes: (i) principles. Chem Phys Lett 379:209

15. Goursot A, Chermette H (1985) Ligand field and Rydberg assignments of the PtCl42− spectrum: a relativistic MS-Xα study. Can J Chem 63:1407

16. Atanasov M, Daul CA, Rauzy C (2004) A DFT Based Ligand Field Theory. Struct Bond 106:97

17. Borel A, Daul CA, Helm L (2004) Hybrid ligand-field theory/quantum chemical calculation of the fine structure and ZFS in lanthanide(III) complexes. Chem Phys Lett 383:584

18. Senn F, Helm L, Borel A, Daul CA (2012) Electronic fine structure calculation of [Gd(DOTA)(H2O)]– using LF-DFT: The zero field splitting. Comptes Rendus de Chimie 15:250

19. Atanasov M, Baerends EJ, Baettig P, Bruyndonckx R, Daul C, Rauzy C, Zbiri M (2004) The calculation of ESR parameters by density functional theory: the g- and A-tensors of Co(acacen). Chem Phys Lett 399:433

20. Atanasov M, Daul CA (2003) A DFT based ligand field model for magnetic exchange coupling in transition metal dimer complexes:: (ii) application to magnetic systems with more than one unpaired electron per site. Chem Phys Lett 381:584

21. Senn F, Daul CA (2010) Calculation of 59Co shielding tensor σ using LF–DFT, THEOCHEM J Mol Struct 954:105

22. Senn F, Zlatar M, Gruden-Pavlovic M, Daul C (2011) Computational analysis of tris(1,2-ethanediamine) cobalt(III) complex ion: calculation of the 59Co shielding tensor using LF-DFT. Monatsch Chem 142:593

23. Ramanantoanina H, Urland W, Cimpoesu F, Daul C (2013) Ligand field density functional theory calculation of the 4f2 → 4f15d1 transitions in the quantum cutter Cs2KYF6:Pr3+. Phys Chem Chem Phys 15:13902

24. Ramanantoanina H, Urland W, Garcia-Fuente A, Cimpoesu F, Daul C (2013) Calculation of the 4f1→4f05d1 transitions in Ce3+-doped systems by Ligand Field Density Functional Theory. Chem Phys Lett 588:260

25. Ramanantoanina H, Urland W, Garcia-Fuente A, Cimpoesu F, Daul C (2014) Ligand field density functional theory for the prediction of future domestic lighting. Phys Chem Chem Phys 16:14625

26. Ramanantoanina H, Urland W, Herden B, Cimpoesu F, Daul C (2015) Tailoring the optical properties of lanthanide phosphors: prediction and characterization of the luminescence of Pr3+-doped LiYF4. Phys Chem Chem Phys 17:9116

27. Ramanantoanina H, Cimpoesu F, Göttel C, Sahnoun M, Herden B, Suta M, Wickleder C, Urland W, Daul C (2015) Prospecting Lighting Applications with Ligand Field Tools and Density Functional Theory: A First-Principles Account of the 4f7–4f65d1 Luminescence of CsMgBr3:Eu2+. Inorg Chem 54:8319

28. Ramanantoanina H, Sahnoun M, Barbiero A, Ferbinteanu M, Cimpoesu F (2015) Development and applications of the LFDFT: the non-empirical account of ligand field and the simulation of the f–d transitions by density functional theory. Phys Chem Chem Phys 17:18547

29. Ramanantoanina H, Kuri G, Daul C, Bertsch J (2016) Core electron excitations in U4+: modelling of the nd105f2 → nd95f3 transitions with n = 3, 4 and 5 by ligand field tools and density functional theory. Phys Chem Chem Phys 18:19020

30. de Groot FMF, Fuggle JC, Thole BT, Sawatzky GA (1990) 2p x-ray absorption of 3d transition-metal compounds: An atomic multiplet description including the crystal field. Phys Rev B 42:5459

31. DeBeer-George S, Petrenko T, Neese F (2008) Prediction of Iron K-Edge Absorption Spectra Using Time-Dependent Density Functional Theory. J Phys Chem A 112:12936

32. Kawai J, Takami M, Satoko C (1990) Multiplet structure in Ni Kβ x-ray fluorescence spectra of nickel compounds. Phys Rev Lett 65:2193

33. Matthew JAD, Strasser G, Netzer F (1983) Multiplet effects and breakdown of dipole selection rules in the 3d → 4f core-electron-energy-loss spectra of La, Ce, and Gd. Phys Rev B 27:5839

34. Ilton ES, Bagus PS (2008) Ligand field effects on the multiplet structure of the U4f XPS of UO2. Surf Sci 602:1114

35. de Groot F (2005) Multiplet effects in X-ray spectroscopy. Coord Chem Rev 249:31

36. Thole BT, Cowan RD, Sawatzky GA, Fink J, Fuggle JC (1985) New probe for the ground-state electronic structure of narrow-band and impurity systems. Phys Rev B 31:6856

37. Radtke G, Lazar S, Botton GA (2006) High-resolution EELS investigation of the electronic structure of ilmenites. Phys Rev B 74:155117

38. Jahn HA, Teller E (1937), Stability of Polyatomic Molecules in Degenerate Electronic States. I. Orbital Degeneracy, Proc R Soc London, Ser A 161:220

39. Bersuker IB (2006) The Jahn-teller effect. Cambridge University Press, Cambridge

40. Yamamoto T (2008) Assignment of pre-edge peaks in K-edge x-ray absorption spectra of 3d transition metal compounds: electric dipole or quadrupole?. X-ray spectrum 37:572

41. Westre TE, Kennepohl P, DeWitt JG, Hedman B, Hodgson KO, Solomon EI (1997) A Multiplet Analysis of Fe K-Edge 1s → 3d Pre-Edge Features of Iron Complexes. J Am Chem Soc 119:6297

42. de Groot F, Vanko G, Glatzel P (2009) The 1s x-ray absorption pre-edge structures in transition metal oxides. J Phys Condens Matter 21:104207

43. Mehadji C, Nour S, Chermette H, Cartier C, Menage S, Verdaguer M (1990) X-ray absorption of tetraoxomanganates (MnO4n−: Experimental and MS LSD computational studies. Chem Phys 148:95

44. Mehdji C, Chermette H, Cartier C, Verdaguer M (1995) X-ray Absorption Near-Edge Structures of Chloroferrates [FeIICl4]2-, [FeIIICl4]-, and [FeIIICl6]3-: Experimental and MS-LSD Computational Studies. J Phys Chem 99:5568

45. Hahn JE, Scott RA, Hodgson KO, Doniach S, Desjardins SR, Solomon EI (1982) Observation of an electric quadrupole transition in the X-ray absorption spectrum of a Cu(II) complex. Chem Phys Lett 88:595

46. Wong J, Lytle FW, Messmer RP, Maylotte DH (1984) K-edge absorption spectra of selected vanadium compounds. Phys Rev B 30: 5596

47. Pantelouris A, Modrow H, Pantelouris M, Hormes J, Reinen D (2004) The influence of coordination geometry and valency on the K-edge absorption near edge spectra of selected chromium compounds. Chem Phys 300:13

48. te Velde G, Bickelhaupt FM, van Gisbergen SJA, Guerra CF, Baerends EJ, Snijders JG, Ziegler T (2001) Chemistry with ADF. J Comput Chem 22:931

49. Guerra CF, Snijders JG, te Velde G, Baerends EJ (1998) Towards an order-N DFT method. Theor Chem Accounts 99:391

50. Baerends EJ, Ziegler T, Autschbach J, Bashford D, Berces A, Bickelhaupt FM, Bo C, Boerrigter PM, Cavallo L, Chong DP, Deng L, Dickson RM, Ellis DE, van Faassen M, Fan L, Fischer TH, Guerra CF, Ghysels A, Giammona A, van Gisbergen SJA, Götz AW, Groeneveld JA, Gritsenko OV, Grüning M, Gusarov S, Harris FE, van den Hoek P, Jacob CR, Jacobsen H, Jensen L, Kaminski JW, van Kessel G, Koostra F, Kovalenko A, Krykunov MV, van Lenthe E, McCormack DA, Michalak A, Mitoraj M, Neugebauer J, Nicu VP, Noodleman L, Osinga VP, Patchkovskii S, Philipsen PHT, Post D, Pye CC, Ravenek W, Rodriguez JI, Ros P, Shipper PRT, Schreckenbach G, Seldenthuis JS, Seth M, Snijders JG, Sola M, Swart M, Swerhone D, te Velde G, Vernooijs P, Versluis L, Vissher L, Visser O, Wang F, Wesolowski T, van Wezenbeek EM, Wiesenekker G, Wolff SK, Woo TK, Yarkolev AL (2014) ADF 2014.01, available at http://www.scm.com

51. Vosko SH, Wilk L, Nusair M (1980) Accurate spin-dependent electron liquid correlation energies for local spin density calculations: a critical analysis. Can J Phys 54:1200

52. Perdew JP, Burke K, Ernzerhof M (1996), - Generalized Gradient Approximation Made Simple, Phys Rev Lett 77:3865

53. Slater JC (1960) Quantum theory of atomic structure, vol I. McGraw-Hill, New York

54. Slater JC (1960) Quantum theory of atomic structure, vol II. McGraw-Hill, New York,

55. Cowan RD (1981) The theory of atomic structure and spectra. Univesity of California Press, Berkeley

56. Griffith JS (1961) The theory of transition-metal ions. Cambridge University Press, Cambridge

57. Lever ABP (1968) Inorganic electronic spectroscopy. Elsevier, Amsterdam

58. Hüfner S (1978) Optical spectra of transparent rare-earth compounds. Academic, New York

59. Ramanantoanina H, Urland W, Cimpoesu F, Daul C (2014) The angular overlap model extended for two-open-shell f and d electrons. Phys Chem Chem Phys 16:12282

60. JØrgensen CK (1962) Absorption spectra and chemical bonding in complexes. Pergamon, Oxford

61. Krause MO, Olivier JH (1979) Natural widths of atomic K and L levels, Kα X-ray lines and several KLL Auger lines. J Phys Chem Ref Data 8:329

62. Ogasawara K, Iwata T, Koyama Y, Ishii T, Tanaka I, Dachi HA (2001) Relativistic cluster calculation of ligand-field multiplet effects on cation L2,3 x-ray absorption edges of SrTiO3, NiO, and CaF2. Phys Rev B 64:115413